Science of the Total Environment 756 (2021) 144130

Contents lists available at ScienceDirect

Science of the Total Environment

journal homepage: www.elsevier.com/locate/scitotenv

Aryl hydrocarbon receptor mediates benzo[*a*]pyrene-induced metabolic reprogramming in human lung epithelial BEAS-2B cells

Guozhu Ye [a,b,*,1], Han Gao [b,c,1], Xu Zhang [b,c], Xinyu Liu [d], Jinsheng Chen [a,b], Xu Liao [b], Han Zhang [b], Qiansheng Huang [a,b,*]

[a] Center for Excellence in Regional Atmospheric Environment, Institute of Urban Environment, Chinese Academy of Sciences, 1799 Jimei Road, Xiamen 361021, China
[b] Key Laboratory of Urban Environment and Health, Institute of Urban Environment, Chinese Academy of Sciences, 1799 Jimei Road, Xiamen 361021, China
[c] University of Chinese Academy of Sciences, 19 Yuquan Road, Beijing 100049, China
[d] CAS Key Laboratory of Separation Science for Analytical Chemistry, Dalian Institute of Chemical Physics, Chinese Academy of Sciences, 457 Zhongshan Road, Dalian 116023, China

HIGHLIGHTS

- 52 metabolites were significantly altered upon BaP exposure and RSV intervention.
- Most amino acids were significantly decreased in BaP-exposed BEAS-2B cells.
- Most fatty acids were significantly increased in BaP-exposed BEAS-2B cells.
- High correlations of AHR signaling with fatty acids and amino acids were observed.
- Fatty acid accumulation was mediated by AHR-PPARA/G-FATP1 signaling.

GRAPHICAL ABSTRACT

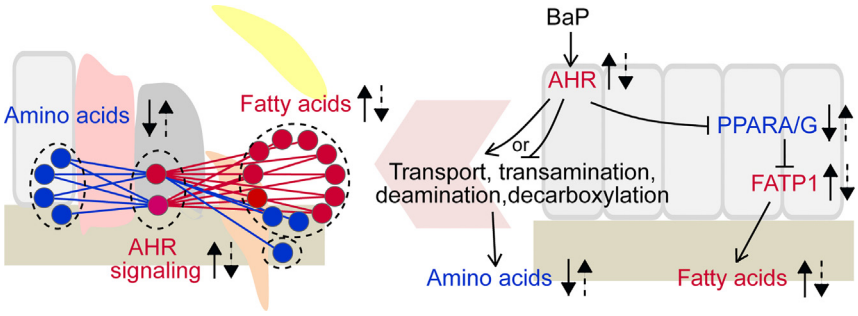

ARTICLE INFO

Article history:
Received 21 July 2020
Received in revised form 9 November 2020
Accepted 21 November 2020
Available online 26 November 2020

Editor: Henner Hollert

Keywords:
AHR
Polycyclic aromatic hydrocarbon
Metabolomics
Amino acid
Fatty acid
Fatty acid transporter FATP1

ABSTRACT

Polycyclic aromatic hydrocarbon exposure accelerates the initiation and progression of lung cancer through aryl hydrocarbon receptor (AHR) signaling. Metabolic reprogramming is a hallmark of cancer. However, how AHR reprograms metabolism related to the malignant transformation in of benzo[*a*]pyrene (BaP)-exposed lung cells remains unclear. After confirming that BaP exposure activated AHR signaling and relevant downstream factors and then promoted epithelial-mesenchymal transition, an untargeted metabolomics approach was employed to discover AHR-mediated metabolic reprogramming and potential therapeutic targets in BaP-exposed BEAS-2B cells. We found that 52 metabolites were significantly altered in BaP-exposed BEAS-2B cells and responsive to resveratrol (RSV) intervention. Pathway analysis revealed that 28 and 30 metabolic pathways were significantly altered in response to BaP exposure and RSV intervention, respectively. Notably, levels of most amino acids were significantly decreased, while those of most fatty acids were significantly increased in BaP-exposed BEAS-2B cells, and above changes were abolished by RSV intervention. Besides, levels of amino acids and fatty acids were highly correlated with those of many metabolites and AHR signaling upon BaP exposure and RSV intervention (the absolute values of Pearson correlation coefficients above 0.8). We further discovered a decrease in peroxisome proliferator-activated receptor (PPAR) A/G signaling and an increase in fatty acid import by the transporter FATP1 in BaP-exposed BEAS-2B cells. Furthermore, inhibition of AHR signaling by CH-223191 abolished BaP-induced repression of PPARA/G signaling and activation of FATP1 in BEAS-2B cells, demonstrating the regulatory role of AHR signaling in fatty acid accumulation via mediating PPARA/G-FATP1 signaling. These data suggested amino acid and fatty acid metabolism, AHR and PPAR-FATP1 signaling as potential therapeutic targets for

* Corresponding authors at: Institute of Urban Environment, Chinese Academy of Sciences, 1799 Jimei Road, Xiamen 361021, China.
E-mail addresses: gzye@iue.ac.cn (G. Ye), qshuang@iue.ac.cn (Q. Huang).
[1] These authors contributed equally to this work.

https://doi.org/10.1016/j.scitotenv.2020.144130

intervening BaP-induced toxicity and related diseases. As far as we known, fatty acid accumulation and high correlations of AHR signaling with amino acid and fatty acid metabolism are novel phenomena discovered in BaP-exposed lung epithelial cells.

1. Introduction

The incidence and mortality of cancer are increasing rapidly worldwide. Lung cancer is the most prevalent cancer (2,093,876 new cases accounting for 11.6% of all cancers in 2018) and the leading cause of cancer death (1,761,007 new cases predicted accounting for 18.4% of all cases in 2018) (Bray et al., 2018). Lung cancer is also the most common cancer with the highest mortality rate in China, and its incidence and mortality account for 18.1% and 24.1% of total cancers, respectively, both well above the world average (Feng et al., 2019). Polycyclic aromatic hydrocarbons, products of incomplete fuel combustion, exist in large quantities in aerosols produced by the combustion of smoking and various fuels, and contribute most to the incidence and development of lung cancer (Guan et al., 2016; Wang et al., 2019). Accordingly, it is of great importance to investigate the exposure effects of polycyclic aromatic hydrocarbons on the incidence and progression of lung cancer.

Exposure to polycyclic aromatic hydrocarbons (such as benzo[*a*]pyrene, BaP) promotes the incidence and progression of lung cancer through aryl hydrocarbon receptor (AHR) signaling (Dietrich and Kaina, 2010; Guerrina et al., 2018; Miller and Ramos, 2001; Zeller et al., 2013). Upon polycyclic aromatic hydrocarbon exposure, cytoplasmic AHR binds with the ligand and enters the nucleus, forming heterodimers with the aryl hydrocarbon receptor nuclear translocator, and binds to the aromatic hydrocarbon response element sequence, thus inducing the transcription of target genes (such as the cytochrome P450 genes, *NRF2* and *RAS*). In addition, bioactive metabolites of polycyclic aromatic hydrocarbons produced via the action of AHR-activated phase I enzymes can form complexes with DNA/proteins to regulate the transcription of target genes, or further conjugate with glucuronic acid, sulfuric acid or glutathione and then be exported outside under the action of phase II and III enzymes, thereby reducing or even eliminating the toxicity. Moreover, AHR can regulate relevant biochemical processes such as phosphorylation via downstream factors, and then activates β-catenin-mediated epithelial-mesenchymal transformation, thus promoting the initiation and progression of lung cancer. Of note, the role of BaP-induced endogenous metabolic changes in the activation of AHR signaling and resultant incidence and progression of lung cancer should not be ignored (Opitz et al., 2011).

Metabolic reprogramming is widely recognized as an important hallmark of cancer, which provides biosynthetic precursors for macromolecules (such as lipids, proteins and nucleic acids), energy substrates and antioxidants for the growth, proliferation and survival of cancer cells, thus contributing to the malignant transformation and progression of lung cancers. Metabolic reprogramming can be driven by oncogenic signals, on the other hand, metabolic alterations can induce changes in oncogene/protein modifications. An amino acid transporter (SLC7A11), importing cysteine while exporting glutamate out of the cells, was found to be overexpressed and associated with worse 5-year overall survival in patients with non-small cell lung cancer (Ji et al., 2018). Overexpression of SLC7A11 promoted proliferation and glutamine dependency in normal airway epithelia cells accompanied by increases in the consumption of cysteine, glutamine and glucose, lactate production, glutamate secretion, basal oxygen consumption rate, maximal respiratory capacity and the glutathione/oxidized glutathione ratio and decreases in reactive oxygen species. Consonantly, SLC7A11 suppression negatively mediated most of above metabolic reprogramming in SLC7A11 overexpressing non-small cell lung cancer cells, and repressed the cell proliferation and tumorigenicity both in vitro and in vivo. Another work revealed that fatty acid metabolic pathway was activated in mutated epidermal growth factor receptor non-small cell lung cancer cells with acquired tyrosine kinase inhibitor resistance, and that pharmacological inhibition of fatty acid synthase suppressed epidermal growth factor receptor palmitoylation and relevant signaling, induced epidermal growth factor receptor ubiquitination, and inhibited tumor growths both in vitro and in vivo (Ali et al., 2018). Therefore, a better and deeper understanding of the metabolic reprogramming in lung cancer would be beneficial to the study of the molecular mechanisms on the initiation and progression of lung cancer and the discovery of potential therapeutic targets.

We previously found that BaP (5 μg/L, around the human blood equivalent dose) exposure promoted the entry of AHR into the nucleus, and activated AHR signaling and its downstream signals (such as K-RAS and β-catenin), thereby inducing the epithelial-mesenchymal transformation and resultant invasion and migration of BEAS-2B cells, and above effects induced by BaP were abolished by resveratrol (RSV, an AHR inhibitor) (Gao et al., 2020). The data demonstrated the regulatory role of AHR signaling in BaP-induced malignant transformation of lung epithelial cells. However, AHR-mediated metabolic reprogramming related to BaP-induced malignant transformation of lung epithelial cells is not clear. Therefore, BEAS-2B cells were exposed to 5 μg/L of BaP to activate AHR signaling and to induce the metabolic reprogramming. Besides, BEAS-2B cells were treated with BaP (5 μg/L) plus RSV (0.1 mg/L) to inhibit AHR signaling and to regulate BaP-induced metabolic reprogramming. Subsequently, an untargeted metabolomics approach based on gas chromatography–mass spectrometry (GC–MS) was employed to discover AHR-mediated metabolic reprogramming and potential therapeutic targets related to BaP-triggered malignant transformation of lung epithelial cells. Furthermore, molecular mechanisms of key metabolic reprogramming mediated by AHR signaling were explored in lung epithelial cells.

2. Materials and methods

2.1. Materials

BaP (96.0%, HPLC grade), dimethyl sulfoxide (≥99.7%), resveratrol (99.0%), CH-223191 (≥98%, HPLC grade), *N*-methyl-N-(trimethylsilyl)-trifluoroacetamide (≥98.5%), pyridine (99.8%) and methoxyamine hydrochloride (98%) were obtained from Sigma-Aldrich (Shanghai, China). Dulbecco's Modified Eagle's medium (high glucose) were purchased from HyClone (USA). Primers were gained from Shanghai Sangon Biotech (Shanghai, China). BEAS-2B cells were ordered from Cell Bank of Chinese Academy of Science (Shanghai, China).

2.2. Cell culture and treatment

BEAS-2B cells were cultured in Dulbecco's Modified Eagle's medium with 10% fetal bovine serum in a humidified incubator containing 5% CO_2 at 37 °C. Five micrograms per liter of BaP, around the human blood equivalent dose, was used to activate AHR signaling and to trigger the metabolic reprogramming in BEAS-2B cells (Cariou et al., 2008; Gao et al., 2020; Song et al., 2013). Moreover, cells were treated with BaP (5 μg/L) plus RSV (0.1 mg/L) for 48 h to inhibit AHR signaling and to mediate BaP-induced metabolic reprogramming in BEAS-2B cells. Furthermore, BEAS-2B cells were exposed to BaP (25 μg/L) and BaP plus CH-223191 (0.5 μg/mL) for 48 h to confirm the regulatory role of AHR in PPARA/G-FATP1 signaling. Dimethyl sulfoxide (*v*/v, 1‰) treatment worked as the control.

2.3. RNA extraction and reverse transcription polymerase chain reaction analysis

TRIzol reagent (Thermo Fisher Scientific, MA, USA) was used to extract total RNA from BEAS-2B cells. BEAS-2B cells were lysed with 1 mL TRIzol at 4 °C. After adding 200 μL chloroform, the cells were fully homogenized and centrifuged for 15 min at 12,000*g* at 4 °C. Then, the supernatant was transferred into a new tube, where isopropyl alcohol was added with the same volume. After thoroughly mixing by shaking up and down, the sample was centrifuged for 15 min at 12,000*g* at 4 °C. Subsequently, the supernatant was discarded, and the sediment was washed with 1 mL 75% ethyl alcohol. The total RNA was then air dried and resuspended with RNAse-free water. The RNA was reverse transcribed to cDNA with PrimeScript™ RT master mix (Takara, Dalian, China). Real-time reverse transcription polymerase chain reaction was analyzed employing SYBR® Premix Ex Taq™ II (Takara, Dalian, China). β-Actin was employed as the internal standard to normalize the mRNA expression. The relative mRNA expression level was determined using the $2^{-\Delta\Delta Ct}$ method. Primers for quantitative polymerase chain reaction analysis were designed based on the NCBI database (Table S1).

2.4. Western blotting

After the treatment, BEAS-2B cells were washed twice with cold phosphate buffered saline and then incubated with the cold cell lysis buffer for 30 min followed by the centrifugation for 15 min at 12,000*g* at 4 °C. The clear supernatant was transferred into a new tube. The total protein concentration was measured using the Bradford protein assay (Bio-Rad, Hercules, CA, USA). Equal amount of protein was firstly separated on 8% or 10% SDS-PAGE gel and then transferred onto a nitrocellulose membrane. The membrane was marked and blocked with 5% milk for 1.5 h at room temperature. Subsequently, the membrane was incubated with diluted (1:1000) primary antibodies at 4 °C overnight, including β-actin, E-CADHERIN, VIMENTIN, AHR, CYP1A1, CD36 and FATP1 (Cell signaling #4970, #3195 and #5741, Abcam #84833, #3368, #133625 and #69458, respectively). After washing three times using Tris-HCL NaCl Tween 20, the membrane was incubated with secondary antibodies at room temperature for 1 h. After that, membranes were washed three times using Tris-HCL NaCl Tween 20, 30 min for each time, and then rinsed with SuperSignal™ Western Blot Enhancer for 1 min. The proteins were detected using Tanon 6100 (Tanon Inc., Shanghai, China). β-Actin was employed as the internal standard to normalize the protein expression.

2.5. Sample collection and preparation for the metabolomics approach

BEAS-2B cells were washed with phosphate buffered saline and gathered using a scraper following cell culture and treatments. After centrifugation at 5,000 rpm for 5 min, cells were frozen in liquid nitrogen and stored at −80 °C for subsequent sample preparation. One thousand microliters of 80% ice-cold methanol were added to the cell sample and vortexed for 1.0 min. The sample was centrifuged at 13,000 rpm for 15 min at 4 °C. Eight hundred microliters of the supernatant were collected and dried in a SpeedVac concentrator (Thermo Scientific, USA). The dried sample was mixed with 50 μL of methoxyamine hydrochloride (20 mg/mL in pyridine) and vortexed for 30 s, followed by the oximation reaction at 37 °C in a water bath for 1.5 h. Forty microliters of *N*-methyl-N-(trimethylsilyl)-trifluoroacetamide were added to the sample and vortexed for 10 s prior to the silylation reaction at 37 °C in a water bath for 1.0 h. After centrifugation at 13,000 rpm for 15 min at 4 °C, the supernatant of the sample was pipetted for subsequent instrumental analysis.

To assess the stability and repeatability of the metabolomics approach, 800-μL aliquots working as quality control samples were prepared by mixing the residual supernatants of all samples. One quality control sample was treated with the same parameters as the other samples every 4 analytical samples during sample drying and derivatization, instrumental analysis and data processing.

2.6. Instrumental analysis for the metabolomics approach

Metabolic profiles of the cell samples were obtained using a GC–MS system (GCMS-QP 2010 plus, Shimadzu, Japan) equipped with an AOC-20i autosampler. The parameters were set according to our previous studies (Ye et al., 2016; Ye et al., 2014; Ye et al., 2012). One microliter of the sample was injected for instrumental analysis. A DB-5 MS capillary column (30 m × 250 μm × 0.25 μm, J&W Scientific Inc., USA) was used for metabolite separation. Helium was used as the carrier gas in constant flow mode. The linear velocity of helium was 40.0 cm/s, and the split ratio was 1:1. The oven temperature was held at 70 °C for 3.0 min, escalated to 300 °C at a rate of 5 °C/min, and then maintained at 300 °C for 10 min. The temperatures of the inlet, ion source and interface were 300, 230 and 280 °C, respectively. Metabolites were ionized in the electron impact (70 eV) mode. The detector voltage was the same as the tuning one. Mass signals (*m/z*, 33–600) were collected in full scan mode using GCMS solution 2.7 (Shimadzu, Japan). The event time and solvent delay time were 0.2 s and 5.5 min, respectively. The retention time of n-alkanes in a light diesel sample, necessary for calculating the retention indices for the metabolites, was gained via GC–MS analysis under the same conditions as the analytical samples.

2.7. Data preprocessing for the metabolomics approach

Raw mass data were transformed into NetCDF format by GCMS solution 4.2 (Shimadzu, Japan) and utilized for peak matching employing XCMS (Smith et al., 2006). Feature ions of the metabolites were provided by the deconvolution of mass signals employing ChromaTOF 4.43 (LECO Corporation, USA). Metabolite identification was conducted mainly according to library search and manual spectral comparisons and further confirmed by available reference standards based on the mass spectra, retention indices and retention time. Each ion peak area of the metabolite was divided by total ion currents and multiplied by 1×10^8, the data were then utilized for the metabolomics analysis.

2.8. Statistical analysis

Principal component analysis and pathway analysis were conducted using MetaboAnalyst 4.0 (Chong et al., 2018). A two-tailed Mann-Whitney *U* test was applied to discover differential metabolites related to BaP-induced metabolic reprogramming using MeV 4.9.0 (Saeed et al., 2006). An independent samples *t*-test was performed to assess differences in the mRNA and protein expression levels among groups employing Statistics 18 (SPSS Inc., Chicago, USA). The statistical significance level was 0.05. The heat map was generated using MeV 4.9.0. Pearson correlation coefficients were used to evaluate the correlations among metabolites and those between metabolites and AHR signaling. Correlation networks were constructed using Cytoscape 2.8.2 (Cline et al., 2007).

3. Results

3.1. AHR mediates BaP-induced disturbances in the metabolic profiling of BEAS-2B cells

Polymerase chain reaction analysis showed that the mRNA expression levels of genes related to AHR signaling (*AHR*, *ARNT* and *HSP90AA1*) and its downstream factors (*CYP1A1*, *K-RAS* and *HIF-1α*) and epithelial-mesenchymal transition (*TWIST1/2*, *SNAIL2*, *β-CATENIN*, *N-CADHERIN*, *FIBRONECTIN* and *VIMENTIN*) were significantly increased, while the mRNA expression levels of *NRF2* and *E-CADHERIN* were significantly decreased in BEAS-2B cells exposed to 5 and 25 μg/L of BaP, respectively (Fig. 1A and B). Western blotting analysis showed that the

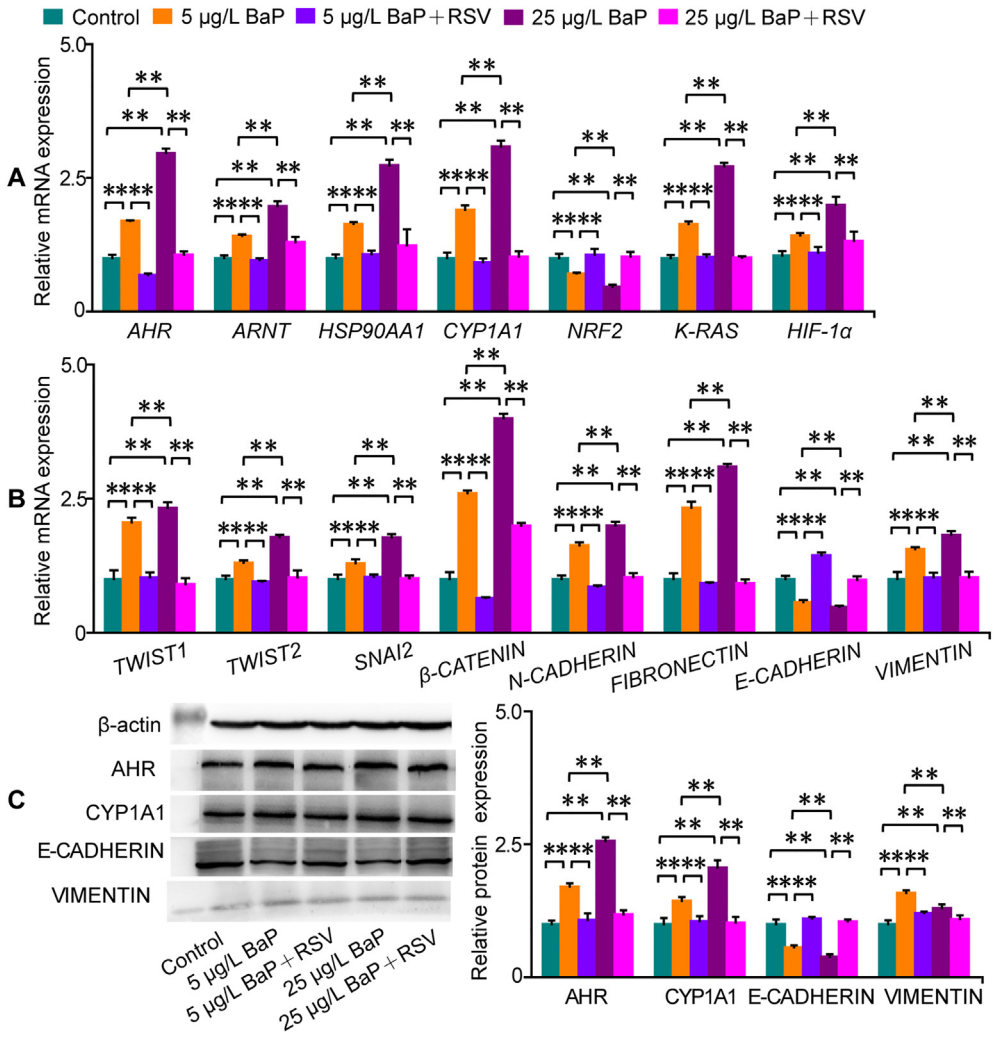

Fig. 1. BaP exposure activates AHR signaling in BEAS-2B cells. Changes in the mRNA expression levels of genes relate to AHR signaling and its downstream factors (A) and epithelial-mesenchymal transition (B) and relevant protein expression levels (C). **, $P < 0.01$, independent samples *t*-test. Columns show the mean plus standard deviation. $n = 4$ biological replicates per group.

protein expression levels of AHR, CYP1A1 and VIMENTIN were significantly increased, while the protein expression level of *E-CADHERIN* was significantly decreased in BEAS-2B cells exposed to 5 and 25 μg/L of BaP, respectively (Fig. 1C). It was noteworthy that there were concentration-dependent effects on BaP-induced changes in AHR signaling and its downstream facts and epithelial-mesenchymal transition, and that above changes induced by BaP exposure could be effectively inhibited or even abolished by RSV intervention. The data demonstrated that BaP exposure activated AHR signaling and relevant downstream factors, thus promoting the malignant transformation of BEAS-2B cells.

Since low concentrations are more conducive to the discovery of early molecular events related to the malignant transformation of lung cells, an untargeted metabolomics approach using GC–MS was employed to reveal AHR-mediated metabolic reprogramming in BEAS-2B cells and to discover potential therapeutic targets upon 5 μg/L of BaP exposure and RSV intervention. It was revealed that the 3 quality control samples were clustered together in the score plot of principal component analysis, and that there were 77.4, 83.9 and 90.0% of the total 4342 total ions in the 3 quality control samples with the relative standard deviations of their contents less than 15, 20 and 30%, respectively (Fig. 2A and B). The data demonstrated that the metabolomics approach had high stability and repeatability (Ye et al., 2019; Ye et al., 2014). We found that the metabolic profiling of the three groups could be clearly distinguished from each other in the score plot of partial least squares discriminant analysis (Fig. 2C). The change in the metabolic profiling of BEAS-2B cells induced by BaP exposure could be effectively mediated by RSV intervention. These data indicated the regulatory role of AHR signaling in the metabolic profiling of BaP-exposed BEAS-2B cells.

3.2. AHR mediates BaP-induced metabolic reprogramming in BEAS-2B cells

Totally, 52 differential metabolites were found using a two-tailed Mann-Whitney *U* test upon BaP exposure and RSV intervention in BEAS-2B cells (Fig. 3 and Table S2). Forty-one of the 52 differential metabolites were confirmed by the reference standards according to the retention time, retention index and mass spectrum. It was clearly observed that metabolites involved in amino acid metabolism, lipid metabolism, carbohydrate metabolism, nucleotide metabolism and other metabolic pathways were significantly altered in response to BaP exposure and RSV intervention (Fig. 3A). Further pathway analysis showed that 28 metabolic pathways were significantly changed in response to BaP exposure in BEAS-2B cells, such as alanine, aspartate and glutamate metabolism, biosynthesis of unsaturated fatty acids, arginine and proline metabolism, linoleic acid metabolism and fatty acid biosynthesis (Fig. 3B). Besides, 30 metabolic pathways were responsive to RSV intervention in BaP-exposed BEAS-2B cells, e.g., arachidonic acid metabolism, biosynthesis of unsaturated fatty acids, fatty acid synthesis,

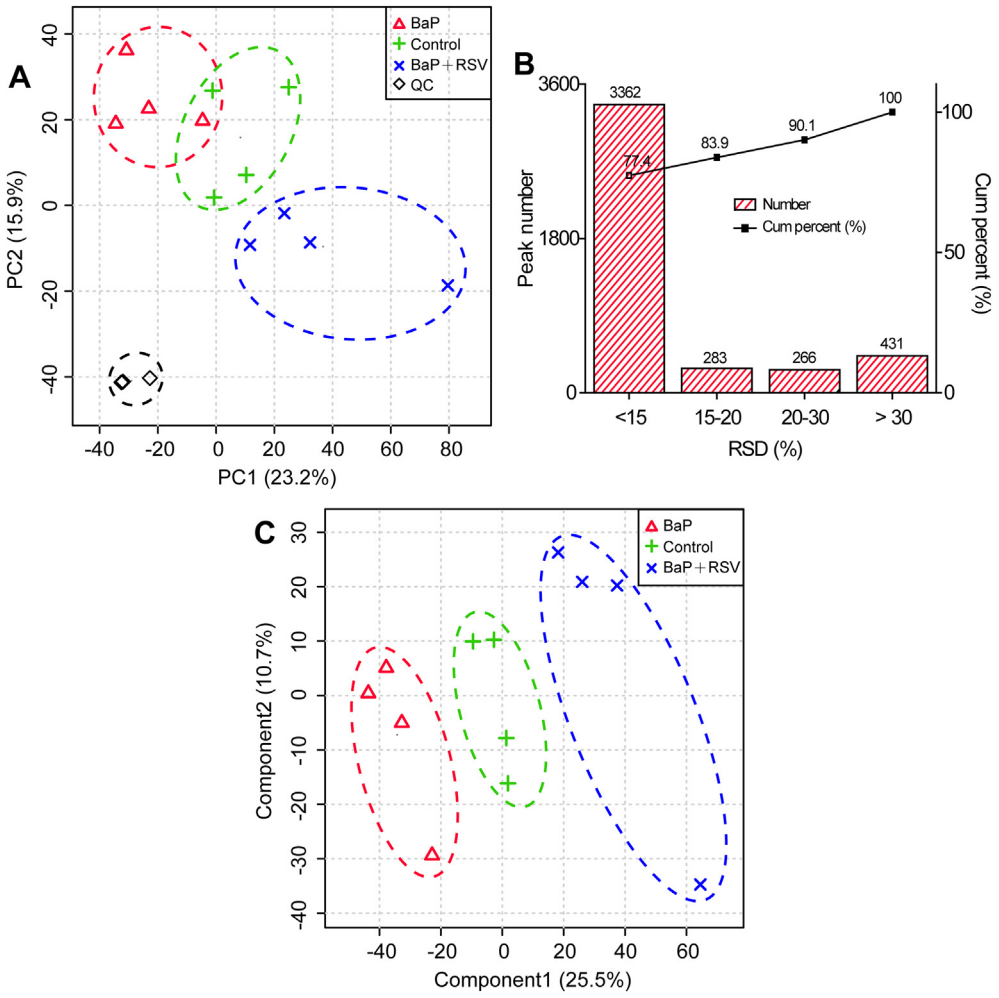

Fig. 2. AHR mediates BaP-induced disturbances in the metabolic profiling of BEAS-2B cells. (A) Quality control (QC) sample distribution in the score plot of principal component analysis. (B) Relative standard deviation (RSD) distribution of metabolite ions in QC samples. (C) Sample distribution in the score plot of partial least squares discriminant analysis.

alanine, aspartate and glutamate metabolism and glycerolipid metabolism (Fig. 3C). Notably, levels of most metabolites related to amino acid metabolism were significantly decreased, while those of metabolites related to lipid metabolism were significantly increased BaP-exposed BEAS-2B cells, and above changes could be effectively alleviated or even abolished by RSV intervention. These data demonstrated the regulatory role of AHR in amino acid and lipid metabolism in BEAS-2B cells. The detailed alterations related to AHR-mediated metabolic reprogramming in BEAS-2B cells are provided below.

3.3. AHR mediates BaP-induced reprogramming of amino acid metabolism in BEAS-2B cells

Amino acids can be used for the synthesis of proteins, nucleotides, lipids, ketone bodies and intermediates of the tricarboxylic acid cycle to support the cell growth and proliferation. It was clear from the heat map plot and pathway analysis that amino acid metabolism, including alanine, aspartate and glutamate metabolism, arginine and proline metabolism, cysteine and methionine metabolism, and valine, leucine and isoleucine metabolism, were significantly altered in response to BaP exposure, and changes in above metabolic pathways were responsive to RSV intervention (Fig. 3). Of note, levels of most metabolites involved in amino acid metabolism, such as aspartate, glutamate, pyroglutamate, methionine and creatinine, were significantly decreased in BaP-exposed BEAS-2B cells, and these effects could be effectively abolished by RSV intervention (Fig. 4). These data indicated the regulatory role of AHR signaling in BaP-induced reprogramming of amino acid metabolism in BEAS-2B cells, such as alanine, aspartate and glutamate metabolism, arginine and proline metabolism, cysteine and methionine metabolism, and valine, leucine and isoleucine metabolism.

3.4. AHR mediates BaP-induced reprogramming of lipid metabolism in BEAS-2B cells

From the heat map plot and pathway analysis, we observed that lipid metabolism were significantly altered in BaP-exposed BEAS-2B cells, including fatty acid biosynthesis, biosynthesis of unsaturated fatty acids, arachidonic acid metabolism, and glycerolipid metabolism, and that changes in most lipid metabolism in BaP-exposed BEAS-2B cells were responsive to RSV intervention (Fig. 3). Notably, levels of 13 fatty acids were significantly increased (such as palmitoleate, linoleate, oleate, arachidonate and docosahexaenoate), while those of cis-11-eicosenoate, trans-11-eicosenoate and eicosanoate were significantly decreased in BaP-exposed BEAS-2B cells (Fig. 5A). The increases in levels of most fatty acids and the decreased level of cis-11-eicosenoate in BaP-exposed BEAS-2B cells were effectively abolished by RSV intervention (Fig. 5A). Above data demonstrated the regulatory role of AHR signaling in fatty acid metabolism in BaP-exposed BEAS-2B cells.

Significant changes in levels of metabolites involved in glycerolipid metabolism were also observed in BEAS-2B cells in response to BaP exposure and RSV intervention (Fig. 5B). The level of glycerol was significantly decreased in BaP-exposed BEAS-2B cells. In addition, RSV intervention significantly decreased levels of 1-monopalmitin, 2-monooleoylglycerol, 1-monooleoylglycerol and 1-monostearin, but

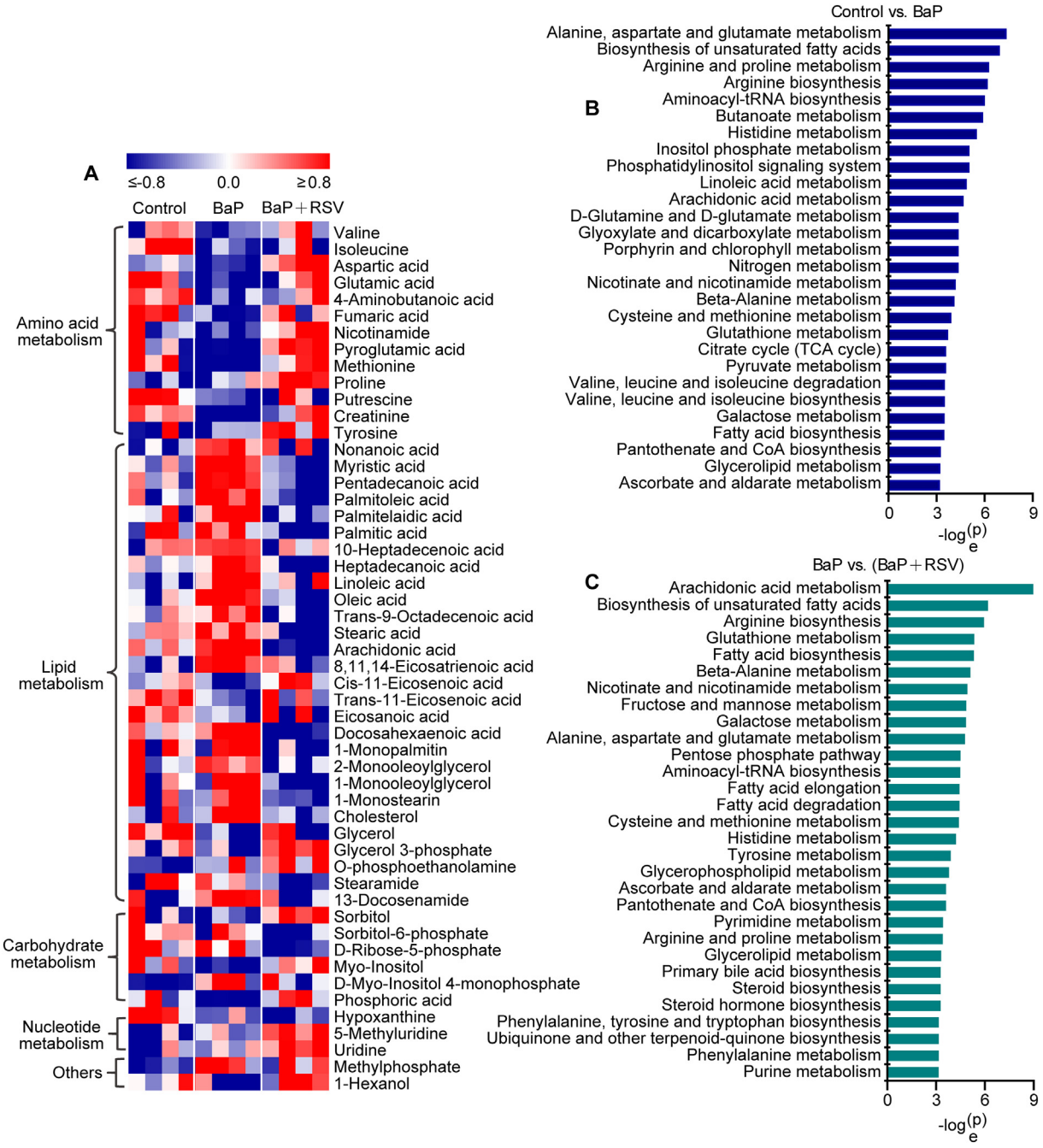

Fig. 3. AHR mediates BaP-induced metabolic reprogramming in BEAS-2B cells. (A) Heat map plot of the metabolic reprogramming in BEAS-2B cells upon BaP exposure and RSV intervention. (B) Metabolic reprogramming in BEAS-2B cells induced by BaP exposure. (C) Metabolic reprogramming in BEAS-2B cells mediated by RSV intervention. $n = 4$ biological replicates per group.

increased the level of glycerol 3-phosphate in BaP-exposed BEAS-2B cells. Above changes in glycerolipid metabolism suggested that the inhibition of AHR signaling accelerated the degradation of monoglycerides.

Alterations of cholesterol metabolism, glycerophospholipid metabolism and fatty amide metabolism were found in response to BaP exposure and RSV intervention in BEAS-2B cells (Fig. 5C). Levels of cholesterol, O-phosphoethanolamine and 13-docosenamide were significantly increased in BaP-exposed BEAS-2B cells, and the increases in levels of cholesterol and 13-docosenamide were effectively abolished by RSV intervention. In addition, RSV intervention significantly decreased the level of stearamide in BaP-exposed BEAS-2B cells. These data indicated the regulatory role of AHR signaling in cholesterol and fatty amide metabolism in BaP-exposed BEAS-2B cells.

3.5. AHR mediates BaP-induced reprogramming of carbohydrate and nucleotide metabolism in BEAS-2B cells

We also found significant changes in carbohydrate metabolism and nucleotide metabolism in response to BaP exposure and RSV intervention in BEAS-2B cells (Fig. S1). Levels of myo-inositol and phosphorate were significantly decreased, while that of myo-inositol 4-phosphate was significantly increased in BaP-exposed BEAS-2B cells. The decreases in levels of myo-inositol and phosphorate in BaP-exposed BEAS-2B cells were effectively abolished by RSV intervention. In addition, RSV intervention increased the level of sorbitol, but increased levels of sorbitol-6-phosphate and ribose-5-phosphate in BaP-exposed BEAS-2B cells. These data demonstrated the involvement of AHR in

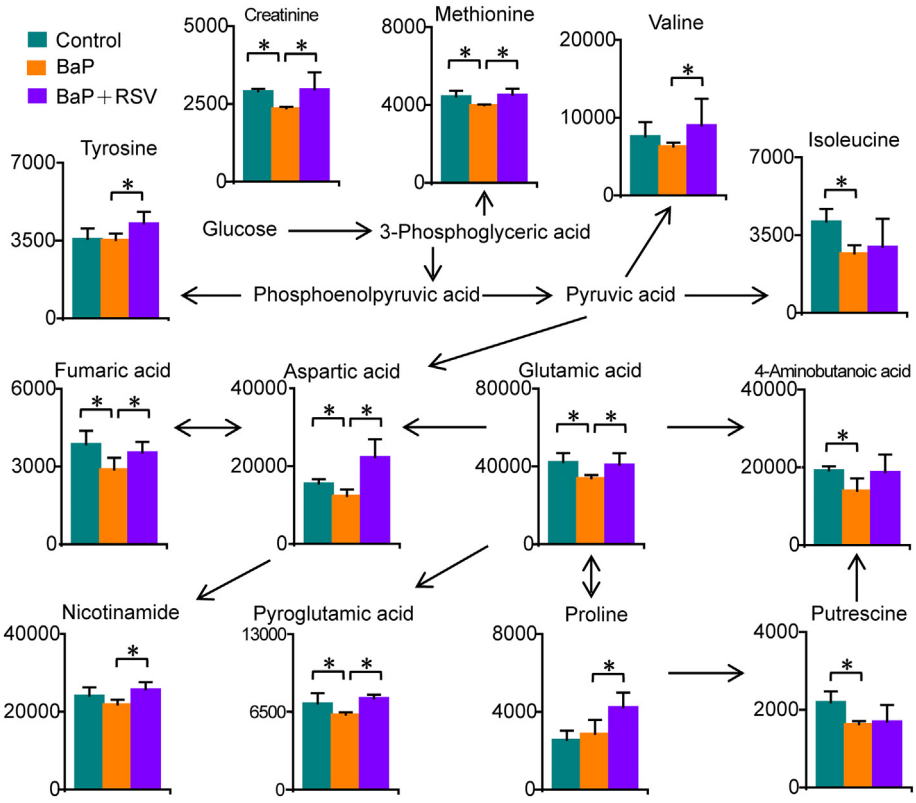

Fig. 4. AHR mediates BaP-induced reprogramming of amino acid metabolism in BEAS-2B cells. *, $P < 0.05$, two-tailed Man-Whitney *U* test. Columns show the mean plus standard deviation. n = 4 biological replicates per group.

carbohydrate metabolism. Moreover, it was observed that the level of hypoxanthine was significantly decreased in BaP-exposed BEAS-2B cells, and that RSV intervention significantly increased levels of 5-methyluridine and uridine in BaP-exposed BEAS-2B cells. The data indicated the involvement of AHR in nucleotide metabolism in BaP-exposed BEAS-2B cells.

3.6. Correlation networks of BaP-induced metabolic reprogramming and AHR signaling

To explore the latent relationships between the metabolic reprogramming and AHR signaling, correlation networks were constructed (Fig. 6). We found that metabolites involved in lipid metabolism (18 fatty acids and 11 other lipids), amino acid metabolism (12 metabolites), carbohydrate metabolism (6 metabolites) and nucleotide metabolites (2 metabolites) were strongly correlated with each other (the absolute value of Pearson correlation coefficient $|C_{ij}| > 0.8$) in BEAS-2B cells upon BaP exposure (Fig. 6A). Similarly, 16 fatty acids, 9 other lipids (not fatty acids), 11 metabolites involved in amino acid metabolism, 4 metabolites involved in carbohydrate metabolism and 3 metabolites involved in nucleotide metabolism had strong correlation with each other ($|C_{ij}| > 0.8$) in BaP-exposed BEAS-2B cells upon RSV intervention (Fig. 6B). The data indicated that lipid metabolism (especially fatty acid metabolism) and amino acid metabolism were at the center of BaP-induced metabolic reprogramming, and that lipid metabolism, amino acid metabolism, nucleotide metabolism and carbohydrate metabolism were correlated with AHR signaling upon BaP exposure and RSV intervention.

To confirmed the correlation of BaP-induced metabolic reprogramming with AHR signaling, correlation networks between the differential metabolites and AHR signaling were built (Fig. 6C–F). We discovered that 16 fatty acids, 5 other lipids (not fatty acids), 10, 3 and 3 metabolites involved in amino acid, carbohydrate and nucleotide metabolism, respectively, were correlated with *AHR* and/or *CYP1A1* in BaP-exposed BEAS-2B cells ($|C_{ij}| > 0.6$, Fig. 6C). Besides, metabolites involved in lipid metabolism (14 fatty acids and 8 other lipids), amino acid metabolism (9 metabolites), carbohydrate metabolism (5 metabolites) and nucleotide metabolism (2 metabolites) were correlated with *AHR* and/or *CYP1A1* in BaP-exposed BEAS-2B cells upon RSV intervention ($|C_{ij}| > 0.6$, Fig. 6D). These data demonstrated the correlation of lipid (especially fatty acid), amino acid, carbohydrate and nucleotide metabolism with AHR signaling in BEAS-2B cells upon BaP exposure and RSV intervention. When the cut off value of $|C_{ij}|$ was set to 0.8, we still found the strong correlations of lipid metabolism (11 fatty acids and 1 other lipid) and amino acid metabolism (4 metabolites) with *AHR* and *CYP1A1* in BEAS-2B cells upon BaP exposure (Fig. 6E). Meanwhile, the strong correlations of lipid metabolism (11 fatty acids and 6 other lipid), amino acid metabolism (4 metabolites) and carbohydrate metabolism (3 metabolites) with *AHR* and *CYP1A1* in BaP-exposed BEAS-2B cells upon RSV intervention could be observed as well ($|C_{ij}| > 0.8$, Fig. 6F). It could be concluded that lipid, amino acid, carbohydrate and nucleotide metabolism were correlated with AHR signaling, and that metabolites involved in lipid metabolism (especially fatty acid metabolism) displayed the closest connections with other metabolites and AHR signaling, followed by those involved in amino acid metabolism. The data suggested the important role of lipid metabolism (especially fatty acid metabolism) in AHR signaling, BaP-induced metabolic reprogramming and related toxicity in BEAS-2B cells.

3.7. AHR mediates BaP-induced fatty acid accumulation in BEAS-2B cells via accelerating the import

Owing to the high correlations of fatty acids with other metabolites and AHR signaling, the mRNA expression levels of fatty acid

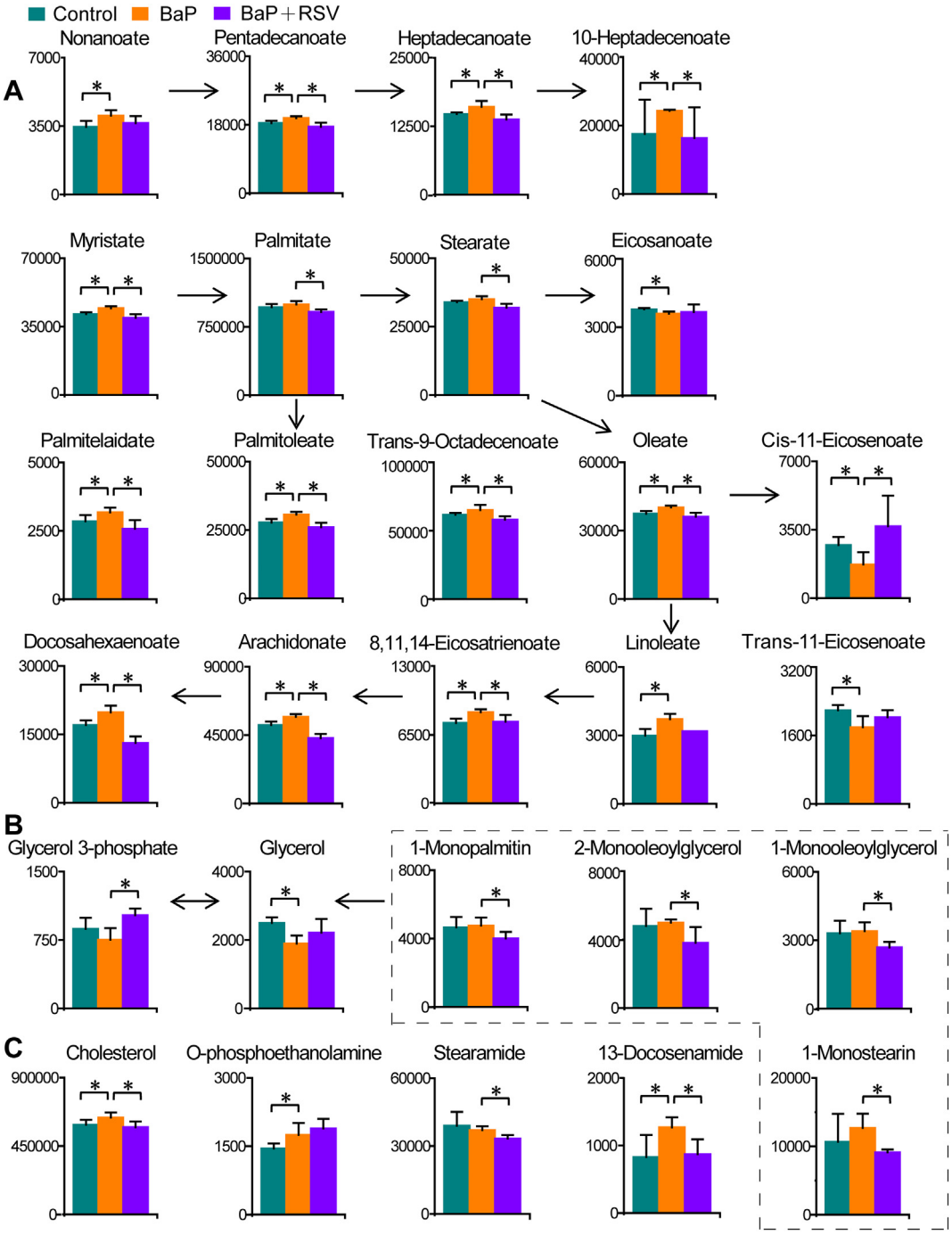

Fig. 5. AHR mediates BaP-induced reprogramming of fatty acid metabolism (A), glycerolipid metabolism (B) and other lipid metabolism (C) in BEAS-2B cells. *, $P < 0.05$, two-tailed Man-Whitney U test. Columns show the mean plus standard deviation. n = 4 biological replicates per group.

transporters were measured to determine how fatty acid accumulation occurred in BaP-exposed BEAS-2B cells (Fig. 7A). It was clear that the mRNA expression levels of *CD36*, *FABP1* and *FATP1* were significantly increased in BEAS-2B cells exposed to 5 μg/L of BaP, and the increased mRNA expression levels of *CD36* and *FATP1* in BaP-exposed BEAS-2B cells were effectively abolished by RSV intervention. To further verify the changes in the mRNA expression levels of *CD36* and *FATP1* induced by BaP exposure at 5 μg/L, BEAS-2B cells were re-exposed to 5 and 25 μg/L of BaP, respectively (Fig. 7B). We found that the mRNA expression levels of *CD36* and *FATP1* were significantly increased in a concentration-dependent manner in BEAS-2B cells after the exposure, and above changes were abolished by RSV intervention. Subsequently, western blotting analysis further confirmed the significant increase in the protein expression level of FATP1 in a concentration-dependent manner, however, there were no significant changes in the protein expression level of CD36 in BEAS-2B cells exposed to 5 and 25 μg/L of BaP, respectively. Moreover, changes in the protein expression level of FATP1 in BaP-exposed BEAS-2B cells were effectively inhibited or even abolished by RSV intention. The data indicated the involvement of fatty acid transporter FATP1 in AHR-mediated fatty acid accumulation in BaP-exposed BEAS-2B cells.

To further examine how BaP exposure activated the mRNA and protein expression levels of FATP1 in BEAS-2B cells, the mRNA expression levels of genes related to peroxisome proliferator-activated receptor (PPAR) signaling, which mediated fatty acid transport, were detected (Fig. 7C). We found that the mRNA expression levels of *PPARA/G* and

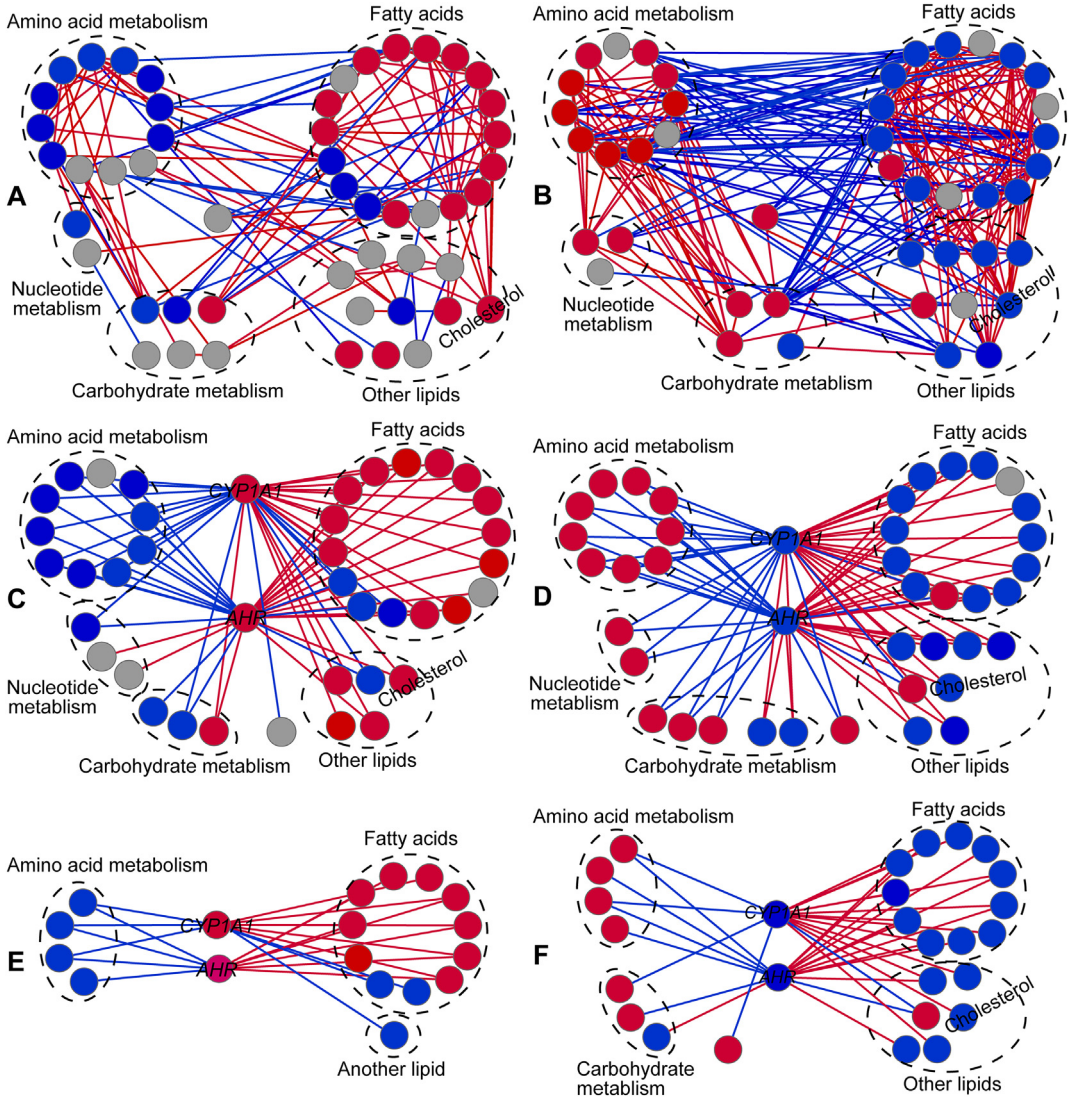

Fig. 6. Correlation networks of BaP-induced metabolic reprogramming and AHR signaling. Red/blue lines, positive/negation correlations; red/blue circles, significantly increased/decreased in the comparison; gray circles, not significantly altered in the comparison. The absolute values of Pearson correlation coefficients between the differential metabolites were greater than 0.8 during BaP exposure (A) and RSV intervention (B). The absolute values of Pearson correlation coefficients between the differential metabolites and AHR signaling were greater than 0.6 during BaP exposure (C) and RSV intervention (D). The absolute values of Pearson correlations coefficients between the differential metabolites and AHR signaling were greater than 0.8 during BaP exposure (E) and RSV intervention (F). $n = 8$ biological replicates per group.

RXRA/G were significantly increased in BaP-exposed BEAS-2B cells, and these effects were effectively abolished by RSV intervention, demonstrating the involvement of PPAR signaling in AHR-mediated fatty acid accumulation. It was revealed that the mRNA expression level of FATP1 was directly regulated by PPARA/G, and that the overexpression of AHR inhibited the activity of PPARs by promoting their ubiquitination degradation (Dou et al., 2019; Pawlak et al., 2015; Ye et al., 2019). Accordingly, the up-regulation of FATP1 expression could be ascribed to the down-regulation of PPARA/G signaling, and the above process was regulated by AHR in BaP-exposed BEAS-2B cells in this study. To confirm our notions, CH-223191 was used to suppress AHR signaling (Fig. 7D). It was clear that inhibition of AHR signaling by CH-223191 abolished BaP-induced repression of PPARA/G signaling and activation of FATP1 and biomarkers of epithelial-mesenchymal transformation in BEAS-2B cells, demonstrating the regulatory role of AHR signaling in PPARA/G-FATP1 signaling and epithelial-mesenchymal transformation. Taken together, AHR mediates BaP-induced fatty acid accumulation in BEAS-2B cells via accelerating the import, which was regulated by PPARA/G-FATP1 signaling.

4. Discussion

Whether in China or the world, lung cancer is the cancer with the highest incidence and mortality (Bray et al., 2018; Feng et al., 2019). Polycyclic aromatic hydrocarbon exposure induces the development of lung cancer via AHR signaling (Dietrich and Kaina, 2010; Guerrina et al., 2018; Miller and Ramos, 2001; Zeller et al., 2013). As a hallmark of cancer, metabolic reprogramming contributes to the malignant transformation and progression of lung cancer (Chen et al., 2019; Hua et al., 2020). However, the mechanism how AHR mediates BaP-induced metabolic reprogramming during the malignant transformation of lung epithelial cells is unclear. Therefore, an untargeted metabolomics approach based on GC–MS was used to uncover AHR-mediated metabolic reprogramming in BaP-exposed BEAS-2B cells and potential therapeutic targets for treating BaP-induced toxicity and diseases. Although changes in levels of relevant metabolites in BEAS-2B cells upon BaP exposure and RSV intervention were not big, there were statistically significant differences. In addition, many metabolites in the same pathway or category had the same changing trend upon BaP

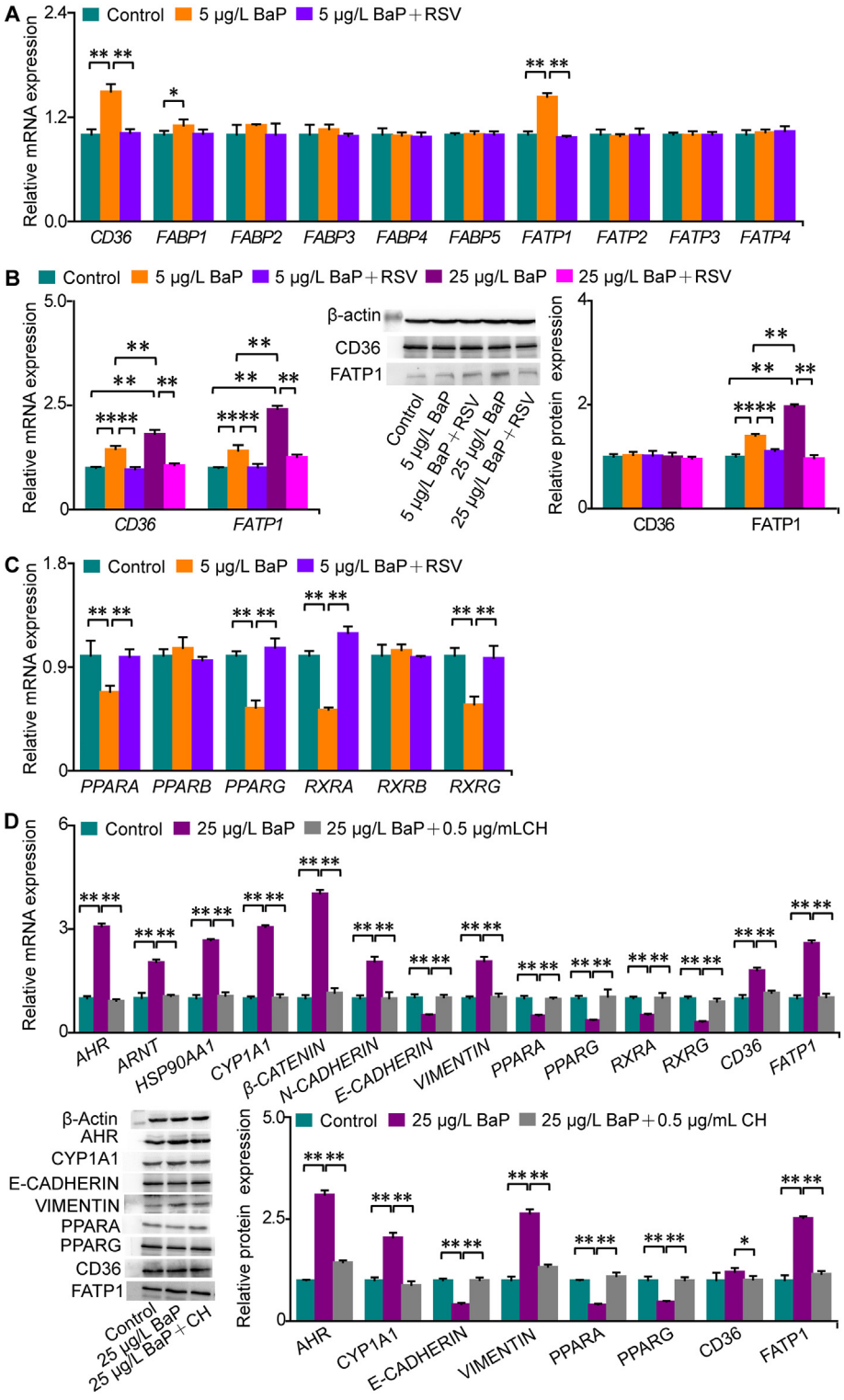

Fig. 7. AHR mediates BaP-induced acceleration of fatty acid transport via PPARA/G-FATP1 signaling in BEAS-2B cells. *, $P < 0.05$, **, $P < 0.01$, independent samples *t*-test. Columns show the mean plus standard deviation. $n = 4$ biological replicates per group. (A, B) AHR mediated BaP-induced acceleration of fatty acid import through activating FATP1. (C) AHR mediated BaP-induced suppression of PPARA/G signaling. (D) Inhibition of AHR signaling by CH-223191 abolished BaP-induced changes in biomarkers of epithelial-mesenchymal transformation and PPARA/G-FATP1 signaling. CH, CH-223191.

exposure and RSV intervention, showing strong regularity. Moreover, we found strong correlations of AHR signaling with amino acid and lipid (especially fatty acid) metabolism upon BaP exposure and RSV intervention, suggesting amino acid and fatty acid metabolism as potential therapeutic targets for intervening BaP-induced toxicity and related diseases.

We found high correlations of amino acids with AHR signaling and other metabolites in BEAS-2B cells upon BaP exposure and RSV intervention in this study. BaP exposure induced significant increases in the expression levels of serum alanine aminotransferase and aspartate aminotransferase and hepatic CYP1A1 in C57BL/6 J mice (Zhu et al., 2020). Hepatic gene expression showed that

2,3,7,8-tetrachlorodibenzo-p-dioxin (a potent AHR agonist) exposure increased the mRNA expression levels of amino acid transporters, while decreased those of antiporters, and that the mRNA expression levels of genes related to the synthesis, oxidation and reduction of glutathione were significantly increased, demonstrating accelerated generation and consumption of glutathione to defense oxidative damages in C57BL/6 mice exposed to 2,3,7,8-tetrachlorodibenzo-p-dioxin (Nault et al., 2016). In addition to supporting glutathione synthesis, amino acid metabolism was also directed to NADPH production to provide reducing equivalents in 2,3,7,8-tetrachlorodibenzo-p-dioxin-exposed mice (Nault et al., 2016). We previously found that the mRNA and protein expression levels of *NRF2* was significantly reduced in BaP-exposed BEAS-2B cells, and these effects were abolished by RSV intervention, demonstrating decreases in nuclear factor-E2-related factor 2-mediated antioxidant capacity and reduced detoxification of bioactive metabolites related to BaP metabolism (Gao et al., 2020). Accordingly, the systematic decreases in levels of most amino acids were probably due to the utilization of amino acids for producing reducing equivalents (NADPH and glutathione) to defense oxidative damages in BaP-exposed BEAS-2B cells (Fader and Zacharewski, 2017; Nault et al., 2016). AHR could directly or indirectly mediate the expression of genes related to the anabolism, catabolism and transport of amino acids, thus affecting amino acid metabolism and relevant physiological functions in BaP-exposed BEAS-2B cells (Nault et al., 2016; Tomblin et al., 2016; Wise et al., 2008).

Here, we also demonstrated high correlations of fatty acids with other metabolites and AHR signaling in BEAS-2B cells upon BaP exposure and RSV intervention. It was demonstrated that hepatic mRNA expression levels of genes related to fatty acid transport (such as *Fabp4*/*5*, *Fatp2* and *Cd36*) were increased, while those of genes related to the synthesis and oxidation of fatty acids (such as *Fasn*, *Acaca*/*b*, *Ehhadh*, *Acsl1*, *Ehhadh* and *Acsm3*) were decreased in mice exposed to 2,3,7,8-tetrachlorodibenzo-p-dioxin (Boverhof et al., 2005; Nault et al., 2016). On the contrary, AHR deficiency increased the mRNA expression of *Ucp1* in brown adipose tissue and mitochondrial β-oxidation genes in muscle in mice (Xu et al., 2015). Moreover, BaP exposure activated AHR signaling, and then induced CYP1A1 expression but decreased PPARA expression in the liver of mice and HepG2 cells, thus leading to liver damages in mice (Zhu et al., 2020). In this study, we found that BaP exposure increased the mRNA and protein expression levels of FATP1, but decreased the mRNA expression levels of *PPARA*/*G* and *RXRA*/*G* in BEAS-2B cells, and that above effects could be abolished by RSV intervention. We previously discovered that activated fatty acid transport by FATP1 led to fatty aid and triglyceride accumulation, which was inhibited or even abolished by both PPARA/G activation and the suppression of FATP1 in oleate-treated macrophages (Ye et al., 2019). Collectively, fatty acid accumulation in BaP-exposed BEAS-2B cells could be ascribed to the accelerated import by FATP1, which was mediated by AHR signaling in this study.

Excessive fatty acids can be used for the synthesis of other lipids with larger molecular weight and bioactive metabolites, thus affecting the activation of AHR and related toxicity. It was showed that BaP exposure triggered triglyceride and total cholesterol accumulation in the serum and liver of mice and HepG2 cells and the formation of lipid droplets in HepG2 cells (Zhu et al., 2020). Other lipid components in lipid droplets, such as phospholipids and sphingomyelins, also accumulated in HaCat cells under BaP exposure (Potratz et al., 2016). It was revealed that enhanced fatty acid uptake by CD36 could be either stored as triglycerides in lipid droplets or oxidized to provide energy currency to support immediate cellular demands, and that the metastasis of cancer cells could be repressed by impeding fatty acid mobilization from lipid droplets (Corbet et al., 2020). On the other hand, imported fatty acids could be used for the synthesis of bioactive metabolites, such as eicosanoids, which could mediate the inflammation, proliferation, invasion, and angiogenesis of cancer cells, and act as ligands for nuclear receptors (Hankinson, 2016; Takeda et al., 2017; Yao et al., 2016).

High correlations of free cholesterol with other metabolites and AHR signaling were observed as well in BEAS-2B cells upon BaP exposure and RSV intervention. It was revealed that 3-methlycholanthrene (an AHR agonist) exposure decreased the mRNA expression levels of *ABCA1* and *LXRA* in HepG2 cells (Iwano et al., 2005). Besides, exposure of human macrophages to 2,3,7,8-tetrachlorodibenzo-p-dioxin and BaP, respectively, decreased the mRNA expression levels of *NPC1*, and induced the accumulation of free cholesterol, cholesteryl esters and neutral lipids assessed by Nile red and oil red O staining, and the decreased mRNA expression level of *NPC1* and lipid accumulation induced by 2,3,7,8-tetrachlorodibenzo-p-dioxin could be abolished by AHR knockdown (Podechard et al., 2009). Accordingly, the increased level of free cholesterol in BaP-exposed BEAS-2B cells could be ascribed to reduced cholesterol efflux, which was mediated by AHR signaling in this study.

5. Conclusions

An untargeted metabolomics approach using GC–MS revealed that AHR mediated changes in levels of metabolites involved in amino acid, lipid, carbohydrate and nucleotide metabolism in BaP-exposed BEAS-2B cells in this study. Notably, levels of most amino acids were significantly decreased, while those of most fatty acids were significantly increased in BaP-exposed BEAS-2B cells, and above changes could be attenuated or even abolished by RSV intervention. High correlations of amino acid and fatty acid metabolism with AHR signaling were found upon BaP exposure and RSV intervention. We further discovered that PPARA/G signaling was suppressed, while the fatty acid import by FATP1 was activated, thus triggering fatty acid accumulation in BaP-exposed BEAS-2B cells, and that above changes were abolished by RSV intervention. These data suggested amino acid and fatty acid metabolism, AHR and PPAR-FATP1 signaling as potential therapeutic targets for intervening BaP-induced toxicity and related diseases. To our knowledge, fatty acid accumulation and high correlations of AHR signaling with amino acid and fatty acid metabolism are novel discoveries in lung epithelial cells.

CRediT authorship contribution statement

Guozhu Ye and Qiansheng Huang conceived and designed this study. Guozhu Ye carried out the metabolomics analysis and data analysis, interpreted the data, wrote and revised the manuscript. Gao Han conducted the cell experiment, polymerase chain reaction analysis and western blotting. Gao Han and Xu Zhang performed the cell sample preparation for the metabolomics analysis. Xinyu Liu deconvoluted the mass data. Xu Liao and Han Zhang initiated the instrumental analysis. Jinsheng Chen checked the manuscript.

Declaration of competing interest

The authors declare that they have no known competing financial interests or personal relationships that could have appeared to influence the work reported in this paper.

Acknowledgements

This work was supported by the Ministry of Science and Technology of the People's Republic of China [grant number 2018YFE0103300]; the Strategic Priority Research Program of the Chinese Academy of Sciences [grant number XDA19050202]; the National Natural Science Foundation of China [grant number 21507128]; and the Natural Science Foundation of Fujian Province [grant number 2018J01020].

Appendix A. Supplementary data

Supplementary data to this article can be found online at https://doi.org/10.1016/j.scitotenv.2020.144130.

References

Ali, A., Levantini, E., Teo, J.T., Goggi, J., Clohessy, J.G., Wu, C.S., et al., 2018. Fatty acid synthase mediates EGFR palmitoylation in EGFR mutated non-small cell lung cancer. EMBO Mol. Med. 10, e8313.

Boverhof, D.R., Burgoon, L.D., Tashiro, C., Chittim, B., Harkema, J.R., Jump, D.B., et al., 2005. Temporal and dose-dependent hepatic gene expression patterns in mice provide new insights into TCDD-mediated hepatotoxicity. Toxicol. Sci. 85, 1048–1063.

Bray, F., Ferlay, J., Soerjomataram, I., Siegel, R.L., Torre, L.A., Jemal, A., 2018. Global cancer statistics 2018: GLOBOCAN estimates of incidence and mortality worldwide for 36 cancers in 185 countries. CA Cancer J. Clin. 68, 394–424.

Cariou, R., Antignac, J.-P., Zalko, D., Berrebi, A., Cravedi, J.-P., Maume, D., et al., 2008. Exposure assessment of French women and their newborns to tetrabromobisphenol-A: occurrence measurements in maternal adipose tissue, serum, breast milk and cord serum. Chemosphere 73, 1036–1041.

Chen, P.H., Cai, L., Huffman, K., Yang, C., Kim, J., Faubert, B., et al., 2019. Metabolic diversity in human non-small cell lung cancer cells. Mol. Cell 76, 838–851.

Chong, J., Soufan, O., Li, C., Caraus, I., Li, S., Bourque, G., et al., 2018. MetaboAnalyst 4.0: towards more transparent and integrative metabolomics analysis. Nucleic Acids Res. 46, W486–W494.

Cline, M.S., Smoot, M., Cerami, E., Kuchinsky, A., Landys, N., Workman, C., et al., 2007. Integration of biological networks and gene expression data using Cytoscape. Nat. Protoc. 2, 2366–2382.

Corbet, C., Bastien, E., Santiago de Jesus, J.P., Dierge, E., Martherus, R., Vander Linden, C., et al., 2020. TGFbeta2-induced formation of lipid droplets supports acidosis-driven EMT and the metastatic spreading of cancer cells. Nat. Commun. 11, 454.

Dietrich, C., Kaina, B., 2010. The aryl hydrocarbon receptor (AhR) in the regulation of cell-cell contact and tumor growth. Carcinogenesis 31, 1319–1328.

Dou, H., Duan, Y., Zhang, X., Yu, Q., Di, Q., Song, Y., et al., 2019. Aryl hydrocarbon receptor (AhR) regulates adipocyte differentiation by assembling CRL4B ubiquitin ligase to target PPARgamma for proteasomal degradation. J. Biol. Chem. 294, 18504–18515.

Fader, K.A., Zacharewski, T.R., 2017. Beyond the aryl hydrocarbon receptor: pathway interactions in the hepatotoxicity of 2,3,7,8-tetrachlorodibenzo-p-dioxin and related compounds. Curr. Opin. Toxicol. 2, 36–41.

Feng, R.M., Zong, Y.N., Cao, S.M., Xu, R.H., 2019. Current cancer situation in China: good or bad news from the 2018 global cancer statistics? Cancer Commun. 39, 22.

Gao, H., Ye, G., Lin, Y., Chi, Y., Dong, S., 2020. Benzo[a]pyrene at human blood equivalent level induces human lung epithelial cell invasion and migration via aryl hydrocarbon receptor signaling. J. Appl. Toxicol. 40, 1087–1098.

Guan, W.J., Zheng, X.Y., Chung, K.F., Zhong, N.S., 2016. Impact of air pollution on the burden of chronic respiratory diseases in China: time for urgent action. Lancet 388, 1939–1951.

Guerrina, N., Traboulsi, H., Eidelman, D.H., Baglole, C.J., 2018. The aryl hydrocarbon receptor and the maintenance of lung health. Int. J. Mol. Sci. 19, 3882.

Hankinson, O., 2016. The role of AHR-inducible cytochrome P450s in metabolism of polyunsaturated fatty acids. Drug Metab. Rev. 48, 342–350.

Hua, Q., Mi, B., Xu, F., Wen, J., Zhao, L., Liu, J., et al., 2020. Hypoxia-induced lncRNA-AC020978 promotes proliferation and glycolytic metabolism of non-small cell lung cancer by regulating PKM2/HIF-1α axis. Theranostics 10, 4762–4778.

Iwano, S., Nukaya, M., Saito, T., Asanuma, F., Kamataki, T., 2005. A possible mechanism for atherosclerosis induced by polycyclic aromatic hydrocarbons. Biochem. Bioph. Res. Co. 335, 220–226.

Ji, X., Qian, J., Rahman, S.M.J., Siska, P.J., Zou, Y., Harris, B.K., et al., 2018. xCT (SLC7A11)-mediated metabolic reprogramming promotes non-small cell lung cancer progression. Oncogene 37, 5007–5019.

Miller, K.P., Ramos, K.S., 2001. Impact of cellular metabolism on the biological effects of benzo[a]pyrene and related hydrocarbons. Drug Metab. Rev. 33, 1–35.

Nault, R., Fader, K.A., Kirby, M.P., Ahmed, S., Matthews, J., Jones, A.D., et al., 2016. Pyruvate kinase isoform switching and hepatic metabolic reprogramming by the environmental contaminant 2,3,7,8-tetrachlorodibenzo-p-dioxin. Toxicol. Sci. 149, 358–371.

Opitz, C.A., Litzenburger, U.M., Sahm, F., Ott, M., Tritschler, I., Trump, S., et al., 2011. An endogenous tumour-promoting ligand of the human aryl hydrocarbon receptor. Nature 478, 197–203.

Pawlak, M., Lefebvre, P., Staels, B., 2015. Molecular mechanism of PPARα action and its impact on lipid metabolism, inflammation and fibrosis in non-alcoholic fatty liver disease. J. Hepatol. 62, 720–733.

Podechard, N., Le Ferrec, E., Rebillard, A., Fardel, O., Lecureur, V., 2009. NPC1 repression contributes to lipid accumulation in human macrophages exposed to environmental aryl hydrocarbons. Cardiovasc. Res. 82, 361–370.

Potratz, S., Jungnickel, H., Grabiger, S., Tarnow, P., Otto, W., Fritsche, E., et al., 2016. Differential cellular metabolite alterations in HaCaT cells caused by exposure to the aryl hydrocarbon receptor-binding polycyclic aromatic hydrocarbons chrysene, benzo[a]pyrene and dibenzo[a,l]pyrene. Toxicol. Rep. 3, 763–773.

Saeed, A.I., Bhagabati, N.K., Braisted, J.C., Liang, W., Sharov, V., Howe, E.A., et al., 2006. TM4 microarray software suite. Method Enzymol. 411, 134–193.

Smith, C.A., Want, E.J., O'Maille, G., Abagyan, R., Siuzdak, G., 2006. XCMS: processing mass spectrometry data for metabolite profiling using nonlinear peak alignment, matching, and identification. Anal. Chem. 78, 779–787.

Song, X.F., Chen, Z.Y., Zang, Z.J., Zhang, Y.N., Zeng, F., Peng, Y.P., et al., 2013. Investigation of polycyclic aromatic hydrocarbon level in blood and semen quality for residents in Pearl River Delta Region in China. Environ. Int. 60, 97–105.

Takeda, T., Komiya, Y., Koga, T., Ishida, T., Ishii, Y., Kikuta, Y., et al., 2017. Dioxin-induced increase in leukotriene B4 biosynthesis through the aryl hydrocarbon receptor and its relevance to hepatotoxicity owing to neutrophil infiltration. J. Biol. Chem. 292, 10586–10599.

Tomblin, J.K., Arthur, S., Primerano, D.A., Chaudhry, A.R., Fan, J., Denvir, J., et al., 2016. Aryl hydrocarbon receptor (AHR) regulation of L-type amino acid transporter 1 (LAT-1) expression in MCF-7 and MDA-MB-231 breast cancer cells. Biochem. Pharmacol. 106, 94–103.

Wang, G.Z., Zhang, L., Zhao, X.C., Gao, S.H., Qu, L.W., Yu, H., et al., 2019. The aryl hydrocarbon receptor mediates tobacco-induced PD-L1 expression and is associated with response to immunotherapy. Nat. Commun. 10 (019-08887).

Wise, D.R., DeBerardinis, R.J., Mancuso, A., Sayed, N., Zhang, X.Y., Pfeiffer, H.K., et al., 2008. Myc regulates a transcriptional program that stimulates mitochondrial glutaminolysis and leads to glutamine addiction. Proc. Natl. Acad. Sci. U. S. A. 105, 18782–18787.

Xu, C.X., Wang, C., Zhang, Z.M., Jaeger, C.D., Krager, S.L., Bottum, K.M., et al., 2015. Aryl hydrocarbon receptor deficiency protects mice from diet-induced adiposity and metabolic disorders through increased energy expenditure. Int. J. Obesity 39, 1300–1309.

Yao, L., Wang, C., Zhang, X., Peng, L., Liu, W., Liu, Y., et al., 2016. Hyperhomocysteinemia activates the aryl hydrocarbon receptor/CD36 pathway to promote hepatic steatosis in mice. Hepatology 64, 92–105.

Ye, G., Zhu, B., Yao, Z., Yin, P., Lu, X., Kong, H., et al., 2012. Analysis of urinary metabolic signatures of early hepatocellular carcinoma recurrence after surgical removal using gas chromatography–mass spectrometry. J. Proteome Res. 11, 4361–4372.

Ye, G., Liu, Y., Yin, P., Zeng, Z., Huang, Q., Kong, H., et al., 2014. Study of induction chemotherapy efficacy in oral squamous cell carcinoma using pseudotargeted metabolomics. J. Proteome Res. 13, 1994–2004.

Ye, G., Chen, Y., Wang, H.O., Ye, T., Lin, Y., Huang, Q., et al., 2016. Metabolomics approach reveals metabolic disorders and potential biomarkers associated with the developmental toxicity of tetrabromobisphenol A and tetrachlorobisphenol A. Sci. Rep. 6, 35257.

Ye, G., Gao, H., Wang, Z., Lin, Y., Liao, X., Zhang, H., et al., 2019. PPARalpha and PPARgamma activation attenuates total free fatty acid and triglyceride accumulation in macrophages via the inhibition of Fatp1 expression. Cell Death Dis. 10, 39.

Zeller, E., Hammer, K., Kirschnick, M., Braeuning, A., 2013. Mechanisms of RAS/beta-catenin interactions. Arch. Toxicol. 87, 611–632.

Zhu, X.-Y., Xia, H.-G., Wang, Z.-H., Li, B., Jiang, H.-Y., Li, D.-L., et al., 2020. In vitro and in vivo approaches for identifying the role of aryl hydrocarbon receptor in the development of nonalcoholic fatty liver disease. Toxicol. Lett. 319, 85–94.